NANO LETTERS

2007
Vol. 7, No. 2
334−337

Enhanced Nonlinear Optical Effects with a Tapered Plasmonic Waveguide

Ewold Verhagen,* Laurens Kuipers, and Albert Polman

Center for Nanophotonics, FOM Institute for Atomic and Molecular Physics (AMOLF), Kruislaan 407, 1098 SJ Amsterdam, The Netherlands

Received October 17, 2006; Revised Manuscript Received December 14, 2006

ABSTRACT

Infrared surface plasmon polaritons (SPPs) are concentrated in a laterally tapered planar Ag waveguide. The near field of SPPs excited with 1490 nm light at a Ag–sapphire interface is probed using the photoluminescence of upconverted Er ions at 550 and 660 nm. SPP interference patterns are observed that exhibit clear evidence of SPP concentration toward the taper end. The concentration leads to an enhancement of the upconversion luminescence intensity from Er energy levels that are populated by multiphoton processes.

The efficient delivery of light to small length scales is a major goal in photonics. The concentration of electromagnetic fields in the smallest possible volume is important in subwavelength guiding, nanolithography, sensing, and data storage. Moreover, large electromagnetic fields allow for the enhancement of nonlinear optical effects.[1,2] One of the routes toward the nanofocusing of light involves surface plasmon polaritons (SPPs): electromagnetic surface waves propagating along a metal−dielectric interface that are coupled to coherent oscillations of the free electrons in the metal.[3] On the one hand, the evanescent character of these modes leads to high field confinements in the direction normal to the metal surface, which can enhance nonlinear processes near the surface.[4] On the other hand, the large wave vectors associated with SPPs offer the possibility of confining these modes also laterally to length scales smaller than the wavelength of light in the bounding dielectric. In view of large field concentrations, the conversion of light to SPPs, their subsequent guiding, and finally their concentration are of fundamental interest. The concentration of propagating SPPs is in competition with losses due to absorption and scattering, which limit the typical propagation lengths of the SPP modes to several tens of micrometers. Several plasmonic waveguiding structures that provide lateral confinement have been shown.[5−9] Finite-width metal stripe waveguides have been studied most thoroughly.[10−14]

Focusing of SPPs has been demonstrated by metallodielectric lenses[15] and corrugations in the metal surface.[16−19] The first indication for SPP concentration in a triangularly shaped termination of a stripe waveguide has been shown by Weeber et al.[11,20] for SPP modes at the air side of a Au waveguide. In a nonplanar geometry, very large field concentrations and asymptotic slowing down of SPPs have recently been predicted to occur at the tip of conical metal waveguides.[21] This has close links to the field enhancements and subwavelength confinement near the tip of gold- or silver-coated fiber tips used in tip-enhanced near-field microscopy, which are also attributed to the generation of SPPs.[22−24]

In this paper, we investigate the enhancement of nonlinear effects due to SPP field concentration in laterally tapered planar Ag waveguides by studying optically active erbium ions as a nonlinear model system. These ions can absorb 1.5 μm light to their first excited state, followed by nonlinear cooperative upconversion and excited-state absorption to populate higher energy levels that emit at 550 and 660 nm.[25,26] The Er ions are implanted in sapphire at close proximity to a silver film. Infrared SPPs are launched along the Ag−sapphire interface by illuminating a subwavelength hole array in the film with a focused beam of 1490 nm laser light. By imaging the upconversion photoluminescence from the Er ions in a confocal microscope, the SPP propagation is visualized, and any upconversion enhancement can be spatially resolved. This luminescence microscopy technique[27,28] allows probing of the field intensity of the purely bound SPP mode propagating along the Ag−sapphire interface, which cannot be readily observed using other methods such as photon scanning tunneling microscopy or leakage radiation microscopy. We observe interference mode patterns on the tapers that clearly show SPP concentration and measure a 4−5 fold enhancement of the 550 nm upconversion photoluminescence intensity near the tip of the waveguide. This work goes beyond experiments in which upconversion enhancement is achieved by field concentration in Kretschmann−Raether geometry[4] by also demonstrating the in-plane focusing of SPPs and the associated locally enhanced upconversion luminescence. It paves the way for the focusing of light to subwavelength length scales.

* Corresponding author. E-mail: verhagen@amolf.nl.

10.1021/nl062440f CCC: $37.00
Published on Web 12/30/2006

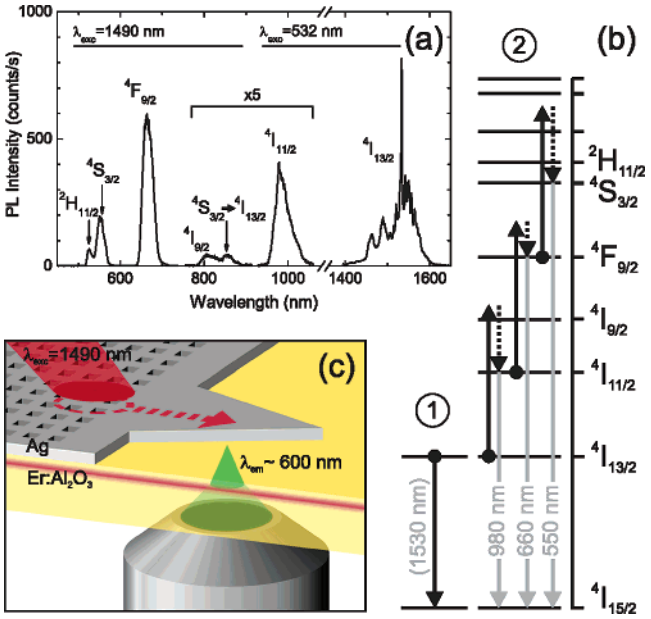

Figure 1. (a) Er photoluminescence spectrum showing emission from different Er levels. For $\lambda_{em} < 900$ nm, the pump wavelength was 1490 nm, whereas for $\lambda_{em} > 900$ nm, 532 nm excitiation light was used. The luminescence signal in the region 750−1100 nm is five times enlarged. (b) Er^{3+} energy level scheme, depicting the cooperative upconversion mechanism that populates higher-order energy levels through energy transfer between two ions excited with 1490 nm light. A multistep upconversion process is shown to reach the levels emitting at 660 and 550 nm. (c) Schematic representation of the measurement principle. SPPs are excited at the Ag−sapphire interface by illuminating a hole array, and Er upconversion luminescence is imaged with a confocal microscope.

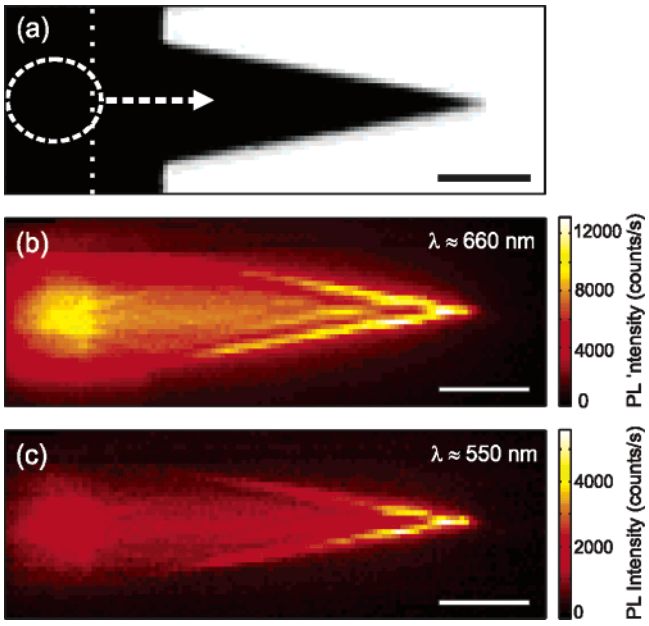

Figure 2. (a) Optical microscopy image of the structure studied, obtained by detecting transmitted 520−570 nm light from a halogen lamp in the confocal microscope. The hole array extends to the left of the dotted line. The dashed circle indicates the position of the excitation spot, and the arrow shows the direction of SPP propagation. (b and c) Spatially resolved photoluminescence maps of Er upconversion emission in the wavelength ranges of 645−690 nm and 520−570 nm, respectively. Both color scales are normalized to the maximum intensity in the field of view. The scale bar is 10 μm.

A 400 μm thick single-crystal sapphire substrate covered with a 10 nm thick Ge conduction layer is implanted with 200 keV Er^+ ions at a fluence of 7×10^{15} cm^{-2}. This dosage results in a peak Er concentration of 2 atom % at a distance of 35 nm to the sapphire surface and a standard deviation in the Gaussian depth distribution of $\sigma = 12$ nm, as simulated with the Monte Carlo program SRIM. After removing the Ge layer, the sample is annealed in vacuum for 1 h at 900 °C. A typical spectrum of the Er photoluminescence from the sample is shown in Figure 1a. The visible part of this emission spectrum ($\lambda_{em} < 900$ nm) is obtained by excitation with 1490 nm laser light from a 45 mW InGaAsP diode laser. The infrared part ($\lambda_{em} > 900$ nm) is recorded with 532 nm excitation light from a 20 mW frequency-doubled Nd:YAG laser. The visible and infrared emission is dispersed by grating spectrographs onto a Si CCD detector and an InGaAs photodiode array detector, respectively. The spectrum is not corrected for variations in pump intensity and collection efficiency of the setup. Comparing the measured spectrum to the level diagram of Er^{3+} depicted in Figure 1b, we see that all excited-state-to-ground-state transitions are observed. All emission that is recorded with the 1490 nm pump is attributed to an upconversion process. In Al_2O_3, the dominant mechanism is cooperative upconversion,[26] depicted schematically in Figure 1b: two Er ions in the first excited-state exchange energy resonantly to promote one to the $^4I_{9/2}$ level. This ion subsequently relaxes quickly to the $^4I_{11/2}$ manifold, from where it can decay either nonradiatively or by the emission of a 980 nm photon. It can also undergo second- and third-order upconversion steps with Er ions in the first or higher excited states to populate even higher energy levels,[25] leading to the observed emission from the $^4F_{9/2}$, $^4S_{3/2}$, and $^2H_{11/2}$ manifolds. In addition, excited-state absorption can also contribute to population of higher energy levels.[26]

Taper and hole array microstructures are fabricated in a 140 ± 5 nm thick Ag film on the sample by electron beam lithography followed by liftoff and are shown schematically in Figure 1c. The Ag is evaporated through resistive heating, and the use of an adhesive layer is avoided, as this layer would be detrimental to SPP excitation and propagation along the Ag−sapphire interface. An optical microscopy image of the structure is shown in Figure 2a. The hole array, with a pitch of 1.46 μm and a hole diameter of roughly 0.6 μm, extends to the left of the dotted line. At a distance of 7 μm from the array, a laterally tapered waveguide of triangular shape is structured in the metal film, with a base width of 12 μm and a length of 36 μm.

SPPs at the smooth Ag−sapphire interface cannot be excited directly with light incident from either dielectric. The hole array is therefore illuminated under such an angle that SPPs excited on the array can couple to the desired propagating SPPs at the Ag−sapphire interface.[29,30] The 1490 nm excitation light is incident from the air side of the film under an angle of 47° with respect to the surface normal to achieve first-order coupling to SPPs at the Ag−sapphire interface, which propagate in the direction indicated by the arrow in Figure 2a. From the angular dependence of the coupling,

the excitation of SPPs at this interface can be confirmed. The p-polarized laser light is focused by a fiber focuser (NA = 0.1) to a 10 μm wide spot near the edge of the array, as depicted in Figure 1c. Er luminescence is collected through the substrate by a 20× objective (NA = 0.75) in a scanning confocal microscope. The collected light passes through a polarizer to avoid distortions due to the birefringence of the sapphire substrate and is transported through a collection fiber to a spectrograph and a Si CCD detector.

The visible upconversion emission is used to determine the two-dimensional distribution of the infrared SPP intensities in the hole array/taper structure. We have shown previously that the bound SPP modes propagating at the high index side of a Ag film can be imaged by detecting the Er photoluminescence emission from the first excited-state at a wavelength of 1530 nm.[27] Here, the resolution of this imaging technique is significantly enhanced by detecting the radiation from higher energy levels of Er ions.[31] In this way, the SPPs excited with 1490 nm light can be probed with wavelengths as short as 550 and 660 nm.

Parts b and c of Figure 2 show upconversion images taken at 645−690 nm ($^4F_{9/2} \rightarrow {}^4I_{15/2}$ transition) and 520−570 nm ($^4S_{3/2}$, $^2H_{11/2} \rightarrow {}^4I_{15/2}$ transitions), respectively. At the left side of the images, Er emission in the excitation spot on the hole array is visible; a SPP beam with a width of ∼10 μm propagates out of this spot across the unstructured Ag before entering the tapered part of the film. Along the taper, a pronounced interference pattern is observed, and the intensity of the upconversion luminescence gradually increases as the taper tip is approached. The relative increase is stronger for the 520−570 nm emission than for the 645−690 nm emission. Note that the intensity in either image is scaled to the maximum intensity in the image, which occurs near the tip of the waveguide in both cases. Along the complete length of the taper, the luminescence intensity is enhanced quite homogeneously near the edge of the waveguide. Outside the taper, the Er luminescence is observed to fade so quickly that a decay length cannot be determined quantitatively given the measurement resolution.

By comparing parts b and c of Figure 2, it can be seen that the positions of the nodes and antinodes in the interference pattern are identical for both emission wavelength ranges. This demonstrates clearly that 1490 nm SPP modes can be precisely imaged using upconversion luminescence in the visible. It proves that the interference pattern is caused by interference of the infrared pump light and that variations due to a possible dependence of the radiative decay rate on the distance from the taper edge are not responsible for this effect. The 2.1 μm separation between the interference fringes that are aligned parallel to the taper edges corresponds to that predicted to arise from the reflections of SPP waves at the edges of the waveguide, considering SPPs excited with 1490 nm light along the Ag−sapphire interface, which are incident at the taper side at a 81° angle. The good visibility of the interference fringes indicates that the reflectivity of the edges is quite large, in accordance with the notion of total internal reflection at the edges. Indeed, the critical angle for such reflections is ∼80°, as estimated from the index

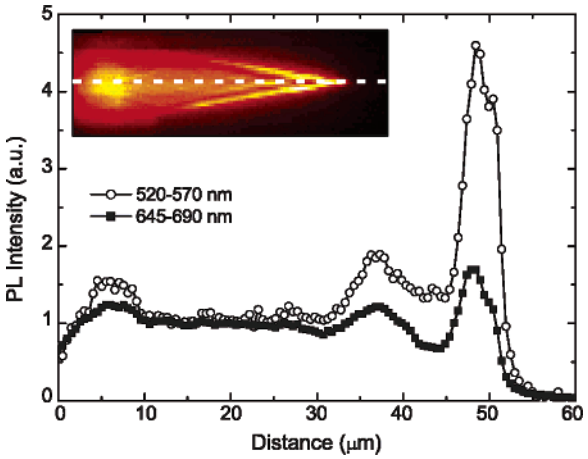

Figure 3. Cross sections of the luminescence microscopy images Figure 2b (closed squares) and Figure 2c (open circles) along the symmetry axis of the tapered waveguide, normalized to the luminescence intensities just outside the hole array.

contrast between the effective refractive index inside the taper (given by the SPP dispersion relation of the mode at the substrate side of the film) and the refractive index of the sapphire substrate outside the taper.[32] We note that it is a priori difficult to make quantitative comparisons between the emission collected from Er ions close to the metal film and that from ions outside the taper. Taking into account local density of states effects,[33] the radiative decay rate near the metal would be reduced and additional nonradiative channels would be introduced. However, redirection of the emitted light due to the metal increases the collected intensity by at most a factor two. Taking both counteracting effects into acount, the maximum possible net increase of collected emission intensity due to the presence of the metal is a factor two. Therefore, we can conclude from the fact that the Er luminescence vanishes quickly outside the waveguide that at the edge of the Ag film SPPs are either efficiently reflected or scattered out in directions away from the Er doped region near the sapphire surface.

Because of reflections of the Gaussian SPP input beam, clear nodes and antinodes would be expected also along the edges of the waveguide. The fact that the Er upconversion luminescence intensity is quite homogeneous along these edges suggests that edge modes could possibly play a role in this structure.[12,13] The focus of the SPP field remains confined to the Ag taper. This behavior is in contrast with what is observed for SPPs propagating at the air side of a Au film on glass.[20] The fact that we find no evidence for leakage across the taper edge may be due to the larger angle of incidence used here, as well as the difference in character between the modes at different sides of the metal film.[14,34] In contrast to the leaky SPP mode residing at the low-index side of a thin metal film, the bound mode propagating at the substrate side of the film has transverse field components that are antiparallel at either side of the metal film. The bound SPP modes studied here are therefore expected to couple to light less efficiently at a sharp film edge.

Figure 3 shows the intensity cross sections of Figure 2b and c taken along the center of the waveguide, normalized

to the respective signal intensities measured at the unstructured metal film just outside the excitation spot. At the tip of the waveguide, a 4−5 fold enhancement of the 550 nm emission and a 1.7 fold enhancement of the 660 nm emission are observed, as compared to the intensity under the smooth film. This clearly demonstrates the effect of SPP concentration in a tapered metal film and the enhancement of the nonlinear upconversion of Er ions due to this concentration. The difference between the two enhancement factors is attributed to the fact that the pump power dependencies of the emission at these two wavelengths are different; the $^4S_{3/2}$ and $^2H_{11/2}$ levels are populated through a higher-order upconversion process than the $^4F_{9/2}$ level. Detailed pump-power dependent emission measurements are required to determine the relative contributions of cooperative upconversion and excited-state absorption for these transitions.[26,35] We note that if the upconversion mechanism is known, a relative measurement of the different upconversion emission intensities is sufficient to determine the *absolute* SPP field intensity at the location of the Er ions. Because the 550 nm emission will scale with the fourth power of the excitation intensity at most,[35] we can estimate a lower limit to the SPP intensity enhancement with respect to the SPP intensity at the start of the taper of roughly 1.5. This demonstrates that the SPP concentration compensates for the losses that occur during propagation along the taper due to absorption and scattering.

Further optimization of the taper geometry should lead to even higher field concentrations in foci significantly beyond the diffraction limit. The bound SPP modes that are studied here possess the necessary requirements for true nanofocusing in tapered SPP waveguides on a planar substrate. By reducing the film thickness at the very end of the waveguide, their dispersion can be tailored to increase the in-plane wave vector and enhance the electromagnetic field at the metal−dielectric interface.[34] The nonlinear detection technique presented here may be of great use to prove and quantify such nanofocusing of optical energy into volumes smaller than the spatial resolution of the measuring device.

In conclusion, we have visualized the excitation, propagation, and concentration of surface plasmon polaritons in laterally tapered silver waveguides. The use of erbium upconversion luminescence provides a unique tool to image the field distributions of infrared SPPs with visible light. Interference effects due to SPP reflection inside the waveguide are observed, and the Er upconversion luminescence is significantly enhanced due to increased field intensities near the end of the waveguide. These results are of interest for the efficient interfacing of micro- and nano-optics and demonstrate the enhancement of nonlinear effects due to SPP field concentration in tapered plasmonic waveguides.

Acknowledgment. This work was made possible by the fabrication and characterization facilities of the Amsterdam nanoCenter. It is part of the research program of the "Stichting voor Fundamenteel Onderzoek der Materie (FOM)", which is financially supported by the "Nederlandse Organisatie voor Wetenschappelijk Onderzoek (NWO)".

References

(1) Chang, R.; Furtak, T. *Surface Enhanced Raman Scattering*; Plenum: New York, 1981.
(2) van Nieuwstadt, J. A. H.; Sandtke, M.; Harmsen, R. H.; Segerink, F. B.; Prangsma, J. C.; Enoch, S.; Kuipers, L. *Phys. Rev. Lett.* **2006**, *97*, 146102, and references therein.
(3) Barnes, W. L.; Dereux, A.; Ebbesen, T. W. *Nature* **2003**, *424*, 824−830.
(4) Baluschev, S.; Yu, F.; Ahl, S.; Yasuda, A.; Nelles, G.; Knoll, W.; Wegner, G. *Nano Lett.* **2005**, *5*, 2482−2484.
(5) Bozhevolnyi, S. I.; Erland, J.; Leosson, K.; Skovgaard, P. M. W.; Hvam, J. M. *Phys. Rev. Lett.* **2001**, *86*, 3008−3011.
(6) Ditlbacher, H.; Hohenau, A.; Wagner, D.; Kreibig, U.; Rogers, M.; Hofer, F.; Aussenegg, F. R.; Krenn, J. R. *Phys. Rev. Lett.* **2005**, *95*, 257403.
(7) Steinberger, B.; Hohenau, A.; Ditlbacher, H.; Stepanov, A. L.; Drezet, A.; Aussenegg, F. R.; Leitner, A.; Krenn, J. R. *Appl. Phys. Lett.* **2006**, *88*, 094104.
(8) Bozhevolnyi, S. I.; Volkov, V. S.; Devaux, E.; Laluet, J.-Y.; Ebbesen, T. W. *Nature* **2006**, *440*, 508−511.
(9) Chen, L.; Shakaya, J.; Lipson, M. *Opt. Lett.* **2006**, *31*, 2133−2135.
(10) Lamprecht, B.; Krenn, J. R.; Schider, G.; Ditlbacher, H.; Salerno, M.; Felidj, N.; Leitner, A.; Aussenegg, F. R. *Appl. Phys. Lett.* **2001**, *79*, 51−53.
(11) Weeber, J.-C.; Krenn, J. R.; Dereux, A.; Lamprecht, B.; Lacroute, Y.; Goudonnet, J. P. *Phys. Rev. B* **2001**, *64*, 045411.
(12) Berini, P. *Phys. Rev. B* **2001**, *63*, 125417.
(13) Weeber, J.-C.; Lacroute, Y.; Dereux, A. *Phys. Rev. B* **2003**, *68*, 115401.
(14) Zia, R.; Selker, M. D.; Brongersma, M. L. *Phys. Rev. B* **2005**, *71*, 165431.
(15) Hohenau, A.; Krenn, J. R.; Stepanov, A. L.; Drezet, A.; Ditlbacher, H.; Steinberger, B.; Leitner, A.; Aussenegg, F. R. *Opt. Lett.* **2005**, *30*, 893−895.
(16) Drezet, A.; Stepanov, A. L.; Ditlbacher, H.; Hohenau, A.; Steinberger, B.; Aussenegg, F. R.; Leitner, A.; Krenn, J. R. *Appl. Phys. Lett.* **2005**, *86*, 074104.
(17) Yin, L.; Vlasko-Vlasov, V. K.; Pearson, J.; Hiller, J. M.; Hua, J.; Welp, U.; Brown, D. E.; Kimball, C. W. *Nano Lett.* **2005**, *5*, 1399−1402.
(18) Liu, Z.; Steele, J. M.; Srituravanich, W.; Pikus, Y.; Sun, C.; Zhang, X. *Nano Lett.* **2005**, *5*, 1726−1729.
(19) Offerhaus, H. L.; van den Bergen, B.; Escalante, M.; Segerink, F. B.; Korterik, J. P.; van Hulst, N. F. *Nano Lett.* **2005**, *5*, 2144−2148.
(20) Krenn, J. R.; Aussenegg, F. R. *Phys. J.* **2002**, *1*, 39−45.
(21) Stockman, M. I. *Phys. Rev. Lett.* **2004**, *93*, 137404.
(22) Koglin, J.; Fisher, U. C.; Fuchs, H. *Phys. Rev. B* **1997**, *55*, 7977−7984.
(23) Janunts, N. A.; Baghdasaryan, K. S.; Nerkararyan, K. V.; Hecht, B. *Opt. Commun.* **2005**, *253*, 118−124.
(24) Bouhelier, A.; Renger, J.; Beversluis, M. R.; Novotny, L. *J. Microsc.* **2003**, *210*, 220−224.
(25) Auzel, F. *Chem. Rev.* **2004**, *104*, 139−173.
(26) van den Hoven, G. N.; Snoeks, E.; Polman, A.; van Dam, C.; van Uffelen, J. W. M.; Smit, M. K. *J. Appl. Phys.* **1996**, *79*, 1258−1266.
(27) Verhagen. E.; Tchebotareva, A. L.; Polman, A. *Appl. Phys. Lett.* **2006**, *88*, 121121.
(28) van den Hoven, G. N.; Polman, A.; van Dam, C.; van Uffelen, J. W. M.; Smit, M. K. *Opt. Lett.* **1996**, *21*, 576−578.
(29) Kim, D. S.; Hohng, S. C.; Malyarchuk, V.; Yoon, Y. C.; Ahn, Y. H.; Yee, K. J.; Park, J. W.; Kim, J.; Park, Q. H.; Lienau, C. *Phys. Rev. Lett.* **2003**, *91*, 143901.
(30) Devaux, E.; Ebbesen, T. W.; Weeber, J.-C.; Dereux, A. *Appl. Phys. Lett.* **2003**, *83*, 4936−4938.
(31) Fragola, A.; Aigouy, L.; de Wilde, Y.; Mortier, M. *J. Microsc.* **2002**, *210*, 198−202.
(32) Zia, R.; Chandran, A.; Brongersma, M. L. *Opt. Lett.* **2005**, *30*, 1473−1475.
(33) Kalkman, J.; Kuipers, L.; Polman, A.; Gersen, H. *Appl. Phys. Lett.* **2005**, *86*, 041113.
(34) Burke, J. J.; Stegeman, G. I.; Tamir, T. *Phys. Rev. B* **1986**, *33*, 5186−5201.
(35) Pollnau, M.; Gamelin, D. R.; Lüthi, S. R.; Güdel, H. U.; Hehlen, M. P. *Phys. Rev. B* **2000**, *61*, 3337−3346.

NL062440F